Second International Symposium on Marine Propulsors
smp'11, Hamburg, Germany, June 2011
Workshop: Propeller performance

Potsdam Propeller Test Case (PPTC)

Olof Klerebrant Klasson[1], Tobias Huuva[2]

[1]Core Competence Team, Berg Propulsion AB, Hönö, Sweden
[2] Core Competence Team, Berg Propulsion AB, Hönö, Sweden

ABSTRACT

The following manuscript describes the methods used, results of and conclusions from the smp'11 Workshop on cavitation and Propeller Performance Case2: Potsdam Propeller Test Case (PPTC).

The purpose of the study was to validate the numerical tools used at Berg Propulsion AB for propeller predictions. The main tools used for the study are the boundary element method PROCAL and the CFD toolbox OpenFOAM.

The analyzed test cases consisted of one open water test, one velocity field measurement and three cavitation cases.

The open water test case resulted in a predicted advance ratio at maximal open water efficiency, $J_{\eta_{Max}}$=1.2, where the open water efficiency η_o= 0.71. One of the main conclusions from this test was that the grid dependence in the used CFD setup was small. The velocity field measurement resulted in an evident tip vortex, which was possible to resolve. The cavitation test resulted in different cavitation patterns and C_p values.

One already known conclusion is that the boundary element method used for the analysis cannot predict pressure side cavitation.

The y+ in the near wall region was larger than 30 for all CFD setups.

Keywords

OpenFOAM; PROCAL; Pressure side cavitation; Validate; Grid dependence;

1 INTRODUCTION

1.1 Background

To achieve better knowledge of the accuracy of a computational tool, it is essential with validation. One excellent way of doing this is to compare between the tool and, not only model tests, but also other tools and setup techniques.

Hence the following submission was made to achieve greater understanding of the computational tools at hand when modeling propellers at Berg Propulsion.

1.2 Objective

The objective of this study is to achieve greater knowledge about the accuracy of the boundary element method PROCAL (PROCAL 2.06) and the CFD toolbox OpenFOAM (OpenFOAM 1.6).

1.3 Method

The method description explains the practice of cases 2.*. The meshes and similar topics are described under this section, but visualized under section 2.

1.3.1 Open Water Tests

A geometry including a propeller gap was used for the analysis of open water performance. The preprocessing tool used for the mesh was ANSA (ANSA 13.10). The geometry was simplified by removing the gap between the hub and the root and the gap in the intersection between hub and shaft, see figure 1.

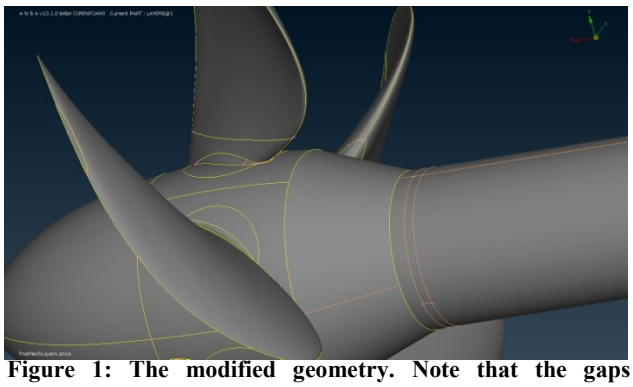

Figure 1: The modified geometry. Note that the gaps between hub and shaft and hub and blade root are filled.

Lines with no connections was pasted together and the tip length at r/R=1.0 was smoothened by a small cut yielding better geometrical representation, see figure 2.

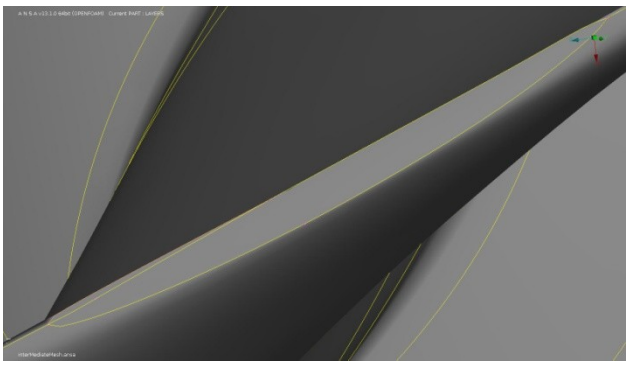

Figure 2: The modification of the tip, where the sharp line shows the new representation and the thinner one the old representation

The blade, hub and shaft were surface meshed with triads. The triads were smaller at high curvature and larger near mid surface sections. For the course mesh, the smallest element length on the surface was 1 mm and the largest 10 mm, resulting in a total of 100000 triad elements.

As turbulence model, a high Reynolds number model of K-omega SST was applied. To model the boundary layer, wall functions were needed. Five prism layers with 1.2 as growth ratio and a starting length of 0.5 mm were applied. For the course mesh, this resulted in 503000 elements.

The rotation was modeled with Multi Reference Frames, MRF. To make use of MRF, a volume surrounding the rotating parts was needed. This volume was made cylindrical with a radius 59 mm larger than the propeller radius. The length of the volume was 69 mm upstream and 2442mm downstream. Within this volume, all parts are rotating. The propeller inside this volume is shown in figure 3.

Figure 3: The propeller inside the MRF-zone

As domain, a larger cylinder was used. This cylinder was made with 1261 mm upstream, 3000 mm downstream and 1261 mm diameter.

The inner volume is, except for being the MRF reference zone, representing the slipstream. The surface of this cylinder was meshed with triads of 1-10 mm. The maximum volume element length was set to 10 mm. The surface of the domain was meshed with 50 mm triads. The maximum volume element length of the domain was set to 75 mm. The interior of both the inner volume and the domain was meshed with hexahedrals, allowing a minimal amount of tetras and pyramids in the transition from the triad surface elements.

The final course mesh resulted in 4.5 million elements for all four blades.

As interpolation schemes, first order accurate schemes were used for the turbulent quantities kinetic energy, inverse turbulent time scale and the turbulent viscosity. For the velocity a second order upwind scheme was applied.

To ensure grid independent results, the mesh was refined at regions with large gradients. The mesh was made larger around shaft and hub, but refined with a factor of two at blade corners and blade tip. The maximum volume element length in the slip stream was also reduced by a factor two. This finer mesh had 151000 surface elements, 605000 prism layer elements and a total amount of 11 million elements for all four blades. The contingent difference between the course and the fine mesh should depend on the discretization error. Since a second order accurate scheme was used, the error would reduce in the order of x^2, if x is the cell length. (Versteeg 2007)

The CFD package used was OpenFOAM (OpenFOAM 1.6) with the solver MRFSimpleFoam. The simulation was of steady Reynolds Averaged Navier-Stokes, RANS, type. The forces and moments were computed on the blades only.

As boundary conditions, the no-slip condition was applied on the surface. The outlet was set as pressure outlet with zero gradient for the remaining quantities. The inlet was set up with uniform velocity inlet and the remaining quantities calculated in accordance with equation 1-4. (Davidsson 2003)

$$k = \frac{3}{2} V_A^2 * I \tag{1}$$

$$\frac{\mu_t}{\mu} = 10 \tag{2}$$

$$\epsilon = \frac{0.09 \rho k^2}{\frac{\mu_t}{\mu}\mu} \tag{3}$$

$$\omega = \frac{\epsilon}{k} \tag{4}$$

Where k = the turbulent kinetic energy; V_A = the advance velocity; I = the turbulent intensity; μ_t = the turbulent viscosity; μ = the fluid viscosity; ϵ = the turbulent dissipation; ρ = the density of the fluid and ω = the specific dissipation.

For the domain, wall functions were used and the pressure was of zero gradient type here.

The results from RANS computations were compared to a boundary element prediction made in PROCAL and the Wageningen series.

1.3.2 Velocity Field Measurement

The velocity field computation was performed in the same way as for the open water test, see section 4.1. The domain and inner volume were rotated and elongated to fit the new arrangement and the longer shaft.

The course mesh had 83000 surface-, 414000 layer- and a total number of 4.6 million elements for all four blades. The corresponding numbers of elements for the fine mesh were 203000, 1015000 and 13.8 million.

To comply with the thrust identity, the speed had to be lowered somewhat. Two different speeds were tested and then the linear relationship between J and K_T was used to find the proper velocity yielding the correct thrust.

1.3.3 Cavitation Tests

For the cavitation analysis the boundary element method PROCAL was used. The analysis was performed by first generating a mesh of quadrilaterals with negligible skewness. A short grid dependence study was performed to ascertain good result quality. A finite tip length was applied to comply with the Kutta-condition. The tip chord fraction was set to 0.6.

For the cavitation free analysis, the number of panels leading edge to trailing edge and root to tip were 30*30. The spacing at leading edge was set to 0.003. The tip spacing was 0.003, the root spacing 0.0078 and the trailing edge spacing 0.00126.

The analyzed number of revolutions was 6 and the number of steps between blades was 12.

The Kutta condition was 0.001 and the jacobian disturbance value was set to 0.0001.

When the Kutta-condition had converged and the radial wake panel and axial force distribution were smooth, the computation was considered converged.

The speeds had to be altered to match the thrust identity. This was done in the same way as for the velocity field measurement, see section 1.3.2.

The atmospheric pressure was computed from the cavitation number using equation 5. (Dyne 2005)

$$p_a = 0.5\rho(nD)^2\sigma_n + p_v - \rho g H \tag{5}$$

Where p_a = the atmospheric pressure; ρ = the fluid density; n = number of revolutions per seconds; D = the propeller diameter; σ = the cavitation number; p_v = the vapor pressure; g = 9.81 m/s^2 and H = the propeller submergence

Finally, a cavitation mesh was set up. When cavitation should be solved in a boundary element method, the solution is very leading edge sensitive. (Bosschers 2009) For this reason, the number of panels leading edge to trailing edge was increased to 70 panels. The number of panels root to tip were decreased to 20. The leading edge spacing was reduced to 0.001.

1.3.4 Post Processing

When the CFD-computations had reached final convergence, they were stopped. Final convergence was considered to be achieved when all residuals of pressure, velocity and turbulent quantities were below 10^{-5}.

The open water diagram was computed from the integrated forces along and moments around the x-axis. Equation 6-8 were used for this purpose. (Dyne 2005)

$$K_T = \frac{T}{\rho n^2 D^4} \tag{6}$$

$$K_Q = \frac{Q}{\rho n^2 D^5} \tag{7}$$

$$\eta_o = \frac{JK_T}{2\pi K_Q} \tag{8}$$

Where K_T = dimensionless thrust; K_Q = dimensionless torque; T = the thrust; Q = the torque; ρ = the fluid density; D = the propeller diameter; n = the number of revolutions per second; η_o = the open water efficiency and J = the advance ratio

The RANS results were post processed in FieldView (FieldView 12). The velocity field was extracted using the sampleDict in OpenFOAM. A cloud of points were picked from the input file demands. The input file requested the tangential, radial and axial velocity at a given ϕ and r/R. ϕ is defined as the angle between dead top centre and current blade position. It is positive in clockwise direction. Hence it can be described by the relationship in equation 9.

$$\phi = tan(\frac{y}{z}) \tag{9}$$

The given radial section can be described in terms of Cartesian coordinates as in equation 10. This is since the equation will yield a cylinder cutting through the given radial section.

$$\frac{r}{R} = \sqrt{\left(\frac{y}{R}\right)^2 + \left(\frac{z}{R}\right)^2} \tag{10}$$

Where r = the radial coordinate and R = the propeller radius

Rewriting gives the Cartesian coordinates as in equation 11 and 12

$$y = arctan(\phi) * z \tag{11}$$

$$z = \frac{r}{\sqrt{tan(\phi)+1}} \tag{12}$$

By sampling the requested points, results of velocity in x, y and z direction were attained. To convert y- and z-direction into radial and tangential velocities the relationship described by equation 13 and 14 were used.

$$V_r = cos(\phi)\, V_z + sin(\phi)\, V_y \qquad (13)$$

$$V_t = cos(\phi)\, V_y - sin(\phi)\, V_z \qquad (14)$$

Where V_r = the radial velocity; V_t = the tangential velocity; V_z = the velocity in z-direction and V_y is the velocity in y-direction

For the cavitaional analysis, the values of C_P were attained at a given radial section by linear interpolation between the nodes. The reason for this was that the nodes that contain the values are located on the cell edges. (Bosschers 2009). To find the radial section requested in the result files, a cylindrical cut was described by the mathematical relationship in equation 10.

Since the boundary element method matches pressures on the blades with the vapor pressure and do not consider vapor content, all cavitation predicted were assumed to have a vapor content of 50%. PROCAL cannot predict pressure side cavitation. (Bosschers 2009) The predicted C_P was calculated, but no pictures of cavitation for case 2.3.3 were presented for this reason.

2 RESULTS

Under this result section, the yielding y+, grid dependence results, velocity plots and similar are presented. The requested input files of case 2.* are attached separately and will not be included here.

2.1 Open Water Tests

The final course and fine mesh for the open water test are visualized with a centre plane cut in figure 4 and 5.

Figure 4: The course mesh for the open water test

Figure 5: The fine mesh for the open water test

The grid dependence comparison from J=0.6 to J=1.2 is presented in table 1. The results are also plotted in figure 6.

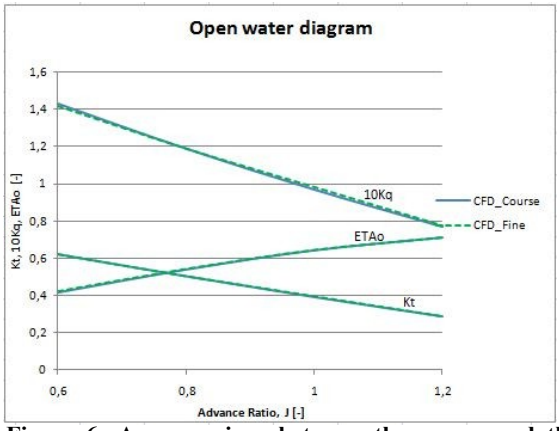

Figure 6: A comparison between the course and the fine mesh for the CFD simulation

Table 1: A comparison between the course and the fine mesh for the open water simulation

J	Kt course	Kt fine	Kq course	Kq fine	ETAo course	ETAo fine
0.6	0.624	0.623	1.431	1.415	0.416	0.421
0.8	0.504	0.505	1.190	1.189	0.540	0.541
1	0.392	0.397	0.970	0.984	0.643	0.643
1.2	0.287	0.289	0.770	0.778	0.712	0.710

The y+ values for the course and the fine mesh is presented in table 2.

Table 2: The y+-value of the course and fine mesh at corresponding advance ratio.

J	y+ course	y+ fine
0.6	34	30
0.8	26	31
1	25	34
1.2	25	34

The axial velocity distribution of the open water test at J=0.6 is visualized in figure 7.

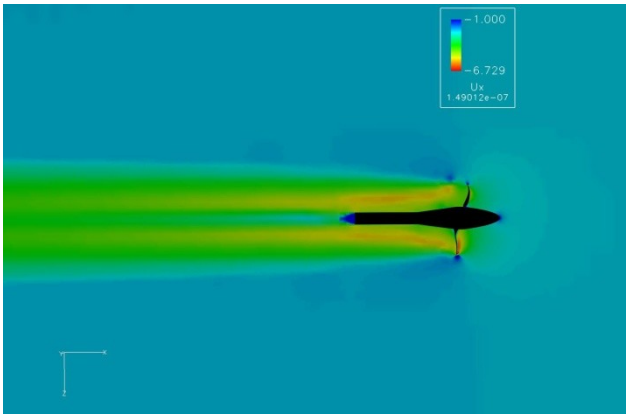

Figure 7: The axial velocity distribution for the open water test at J=0.6

The pressure distribution of the blades and hub in the open water test at J=0.6 is visualized in figure 8.

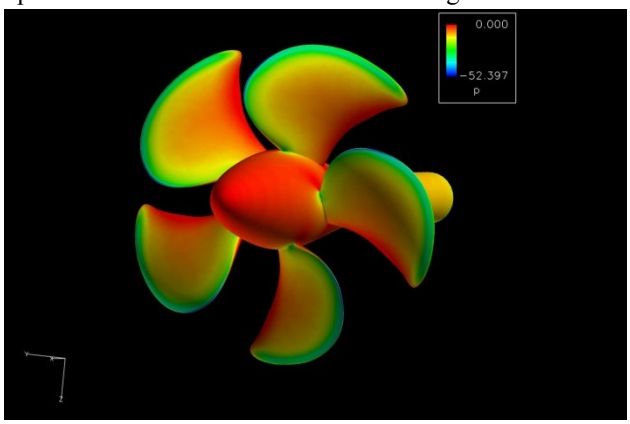

Figure 8: Pressure distribution of the suction side from the open water test at J=0.6

The open water test results of the CFD are compared to results from PROCAL and the Wageningen series in figure 9.

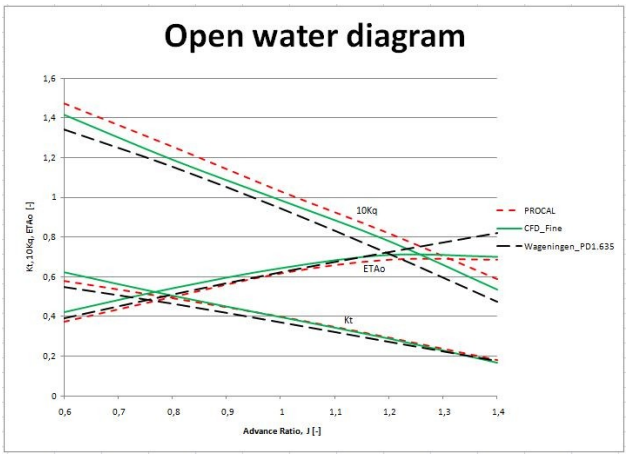

Figure 9: Open water curves from Wageningen, PROCAL and the fine CFD results

2.2 Velocity Field Measurement

The fine mesh used in the velocity field measurement is shown in figure 10.

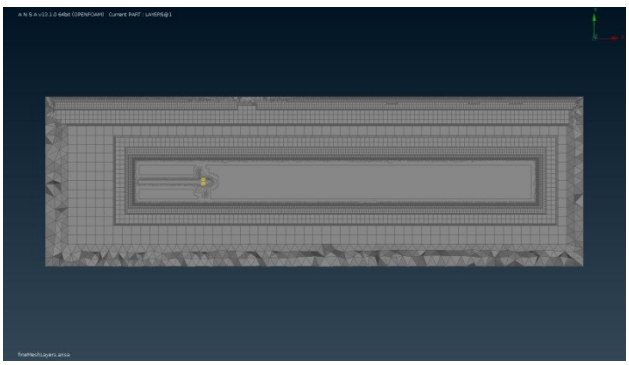

Figure 10: The fine mesh used for the velocity field measurement

The velocity, corresponding K_T and corresponding y+ are tabulated in table 3. The results are from the fine mesh.

Table 3: Velocities and corresponding J, K_T and y+ for the fine mesh of the velocity field measurement.

Va	J	Kt	y+
7.204	1.253	0.248	89
7.187	1.250	0.249	89

$V_A = 7.1867$ was chosen as working point.

In figure 11 an iso-surface with helicity of 150 m^2/s^2 is shown to visualize the generated tip vortex. The axial velocity field is shown in figure 12. Figure 13 shows the pressure distribution of the propeller suction side.

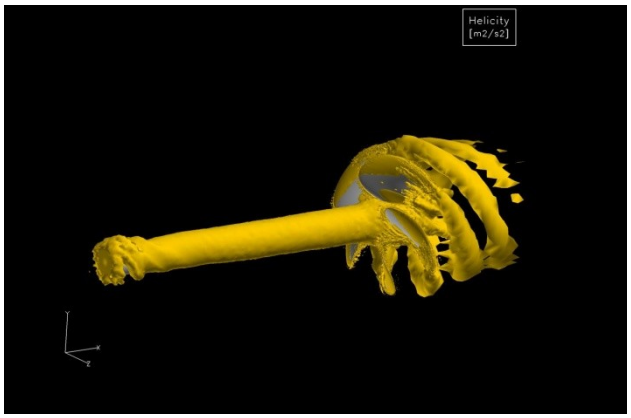

Figure 11: Tip vortex with helicity of 150 m^2/s^2 at the working point

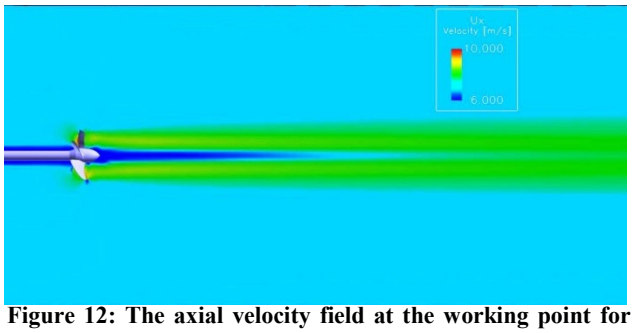

Figure 12: The axial velocity field at the working point for the velocity field measurement

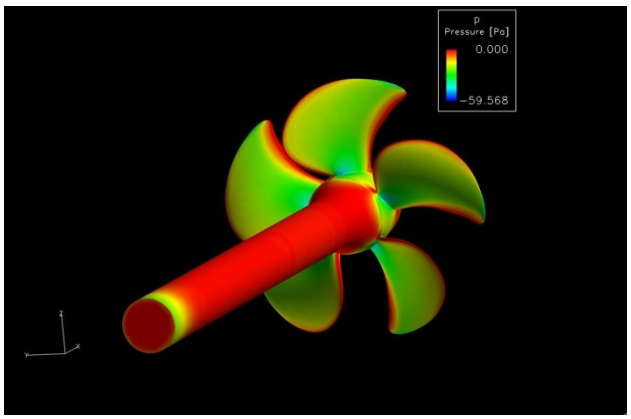

Figure 13: Pressure distribution of the suction side at the working point for the velocity field measurement

2.3 Cavitation tests

The non-cavitating mesh used for finding the thrust identity is shown in figure 14. The cavitation mesh is shown in figure 15.

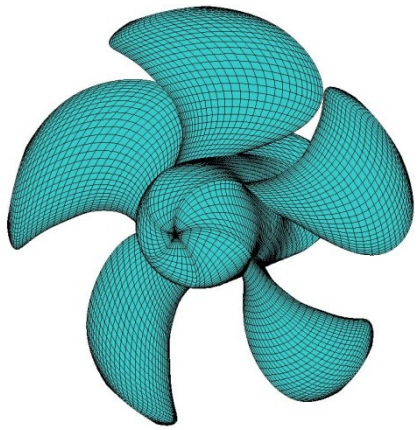

Figure 14: The non cavitating mesh for the cavitational analysis

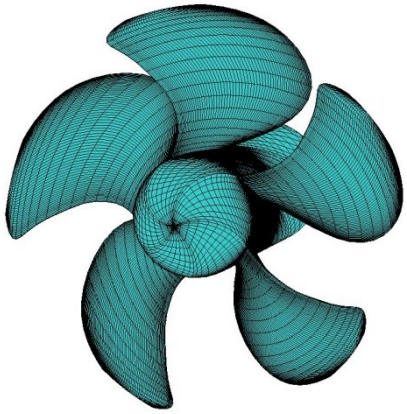

Figure 15: The cavitation mesh for the cavitational analysis

The velocity, corresponding J and resulting K_T to fulfill the thrust identity are tabulated in table 4. This is for a cavitation free computation.

Table 4: Velocities, corresponding J and corresponding K_T to fulfill the thrust identity of the cavitation free condition.

Case	Va	J	Kt
2.3.1	6.269	1.004	0.387
2.3.2	7.986	1.278	0.245
2.3.3	8.987	1.437	0.167

The radial axial force and wake strength distribution at $\phi = 0$ for case 2.3.1 are shown in figure 16 and 17. The same distributions, but for case 2.3.2 and 2.3.3 are shown in figure 18-21.

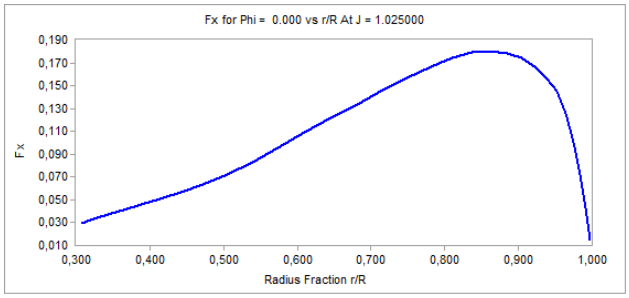

Figure 16: Radial axial force distribution at $\phi = 0$ for case 2.3.1

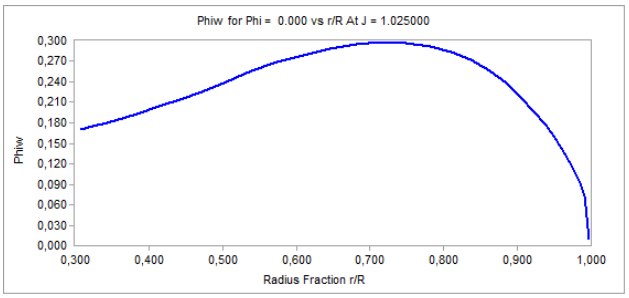

Figure 17: Radial wake strength distribution at $\phi = 0$ for case 2.3.1

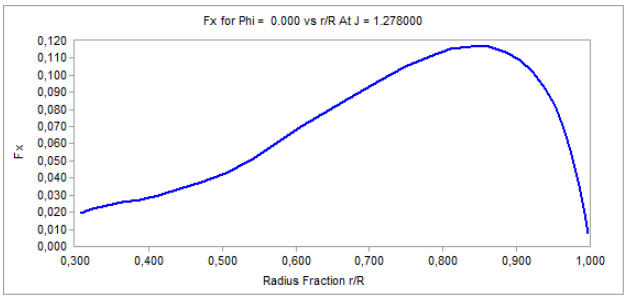

Figure 18: Radial axial force distribution at $\phi = 0$ for case 2.3.2

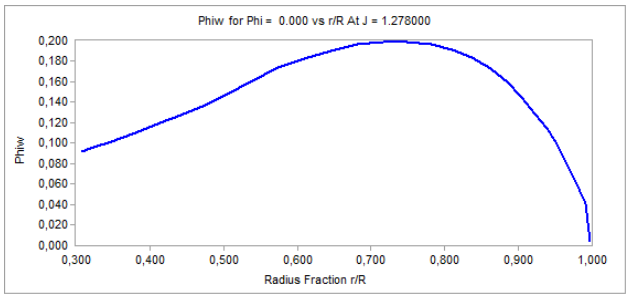

Figure 19: Radial wake strength distribution at $\phi = 0$ for case 2.3.2

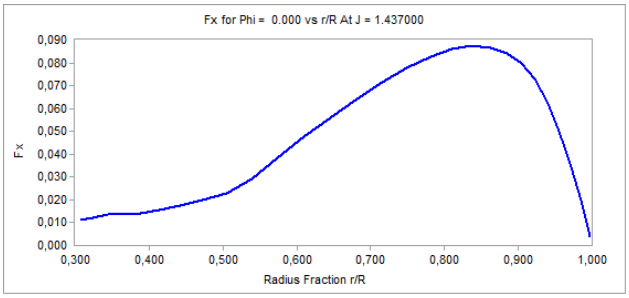

Figure 20: Radial axial force distribution at $\phi = 0$ for case 2.3.3

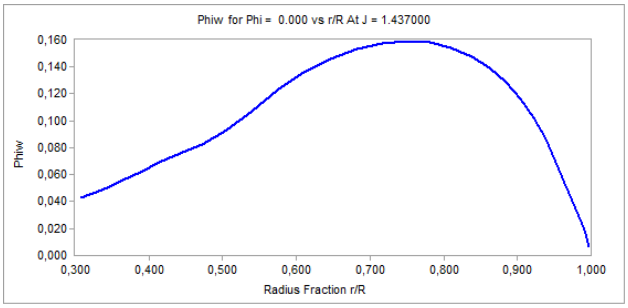

Figure 21: Radial wake strength distribution at $\phi = 0$ for case 2.3.3

The zero degree position is characteristic for the rest of the radial results, which hence would be inadequate to include.

3 CONCLUSIONS

The open water test CFD results are reliable. This can be said knowing that the Results are similar to the PROCAL and the Wageningen prediction. The K_Q is higher from the PROCAL simulation compared to the CFD, but this is a known delimitation of the software. The Wageningen propeller has a smaller hub size, and for that reason a different geometry, since the blade area is the same. The geometry would also differ in terms of profile camber and pitch distribution. This results in lower K_Q and K_T. The CFD-results has been accurate in comparison to model tests before.

The y+ is larger than 30 and smaller than 100 for all simulations, which is preferable when wall functions are used. (Versteeg 2007) This is valid for both the open water simulation and the velocity field measurement.

The discretization error in the computations is small. If we study K_T at J=0.6 and J=0.8 in table 1 e.g. The differences between the points from the course and the fine mesh are:

$$e_{J=0.6} = 0.623578 - 0.623343 = 0.000235$$

$$e_{J=0.8} = 0.504418 - 0.505314 = -0.000896$$

This is very small differences. Reducing the mesh size even further would give almost no noticeable effect. As previously stated, the error is reduced by the decrease in cell length squared. The discretization error must be very small already at the course mesh for this reason.

The velocity field evaluation gives results that look intuitive. A tip vortex is generated, the solution look symmetrical and the K_T matches the thrust identity with a very slight velocity change. The resolution further downstream in the slip stream could be improved, resolving the tip vortex even further.

If the vorticity is studied, it dies out rather quickly, which could be avoided if the large gradients wasn't evened out to the extent they are in this computation. The reason for this is the restriction in computational power. With more CPU cores and more random access memory it would of course be possible to analyze with more cells. This should have a small effect on the velocity field at 0.1D and 0.2D upstream and downstream the propeller disc, where the cell length is very small, though.

If a fully hexahedral mesh would be applied and the wall would be entirely resolved, the results could be improved even further. The reason for not doing this is that the program is used for commercial purposes. Making such a mesh and resolving the wall is too time-consuming.

The cavitational analysis should be reliable for the first and the second case. This can be concluded since the computations are converged with no problem and showing a cavitation pattern that is stable.

The third case should be handled with care, since pressure side cavitation cannot be predicted in PROCAL.

REFERENCES

Versteeg, H.K. & Malalasekera, W. (2007) 'An Introduction to Computational Fluid Dynamics The Finite Volume Method' 2nd ed, Harlow, England

Davidsson, L (2003) 'An introduction to turbulence models'. Department of Thermo and Fluid Dynamics, Chalmers University of Technology, Göteborg, Sweden

Dyne, G. & Bark, G. (2005). 'Ship Propulsion'. Shipping and Marine Technology, Division of Hydrodynamics, Chalmers University of Technology, Göteborg, Sweden

Bosschers, J. (2009) 'PROCAL v2.0 User Guide', Maritime Research Institute, Wageningen, Netherlands

PROCAL 2.06 – a boundary element method for steady and unsteady propeller computations with or without cavitation developed for CRS. It includes both pre and post processor and solver.

OpenFOAM 1.6 – an open source CFD toolbox

ANSA 13.10 – a preprocessing tool for geometry manipulation and mesh-generation for CFD and FEM-computations

FieldView 12 – a standalone postprocessor for OpenFOAM